Research Article Vol. 33, No. 8 / 21 Apr 2025 / Optics Express 18161
Optics EXPRESS

Dual-comb polarization-multiplexing ring-cavity fiber laser for ranging applications

ALBERTO RODRIGUEZ CUEVAS,[1,*] DMITRII STOLIAROV,[1] HANI KBASHI,[1] AND SERGEY SERGEYEV[1]

[1]Aston Institute of Photonic Technologies, College of Engineering and Physical Sciences, Aston University, B4 7ET Birmingham, UK
[*]arc28@alumnos.unican.es

Abstract: We present the design and implementation of a dual-comb polarization-multiplexing ring-cavity fiber laser system tailored for precision ranging applications. This system generates two optical frequency combs within the same cavity enabling enhanced short-term and long-term stability with reduced common noise, while it maintains coherence for more than 125 hours without external stabilization. Also, results show a precision of 340 µm for a 10 ms averaging time with an ambiguity range of 3.8 m. This study confirms the potential of dual-comb polarization-multiplexing systems as a robust and cost-effective solution for precision metrology, LIDAR, and fiber-optic sensing applications.

1. Introduction

Since their complete stabilization [1–4], optical frequency combs have been used in metrology applications. In many of these applications, two pulse trains with slightly different periods t and t+Δt, e.g. two spectra with lines spaced with the repetition rates f and f + Δf are used. The beating of the two optical combs generates a third RF comb linearly mapped to the optical frequency spectrum by a scaling coefficient of f/Δf and spaced by Δf. This approach provides a high precision capability using a very short sampling time [5–8]. In the majority of the cases, the dual-comb is based on two lasers with stabilized repetition rates f_{rep} and carrier-envelope offset frequencies f_{CEO}, in some other cases both frequency combs are self-referenced [9,10]. Nonetheless, either of those stabilization techniques imply a high level of complexity and also a high cost. To address this issue, the generation of both combs in the same cavity has been proposed recently [11]. And at the moment, there is a strong research effort to achieve stabilities and capabilities to a level where this technology become useful for precision applications.

Employing two optical frequency combs generated within a single cavity presents substantial advantages compared to utilizing two independent comb systems [11]. The primary benefit arises from the intrinsic correlation between the combs, as they share identical cavity-induced perturbations. Typically, both short-term frequency jitter and long-term frequency drift in laser oscillators originate predominantly from mechanical vibrations, thermal expansions, environmental noise, and other external disturbances that alter the effective cavity length (L). By generating both combs within a common cavity, such length fluctuations uniformly impact both combs. Consequently, while individual repetition rates (f_{rep}) and carrier-envelope offset frequencies (f_{CEO}) of free-running combs may exhibit temporal drift, the differential quantities Δf_{rep} and Δf_{CEO} between the two combs maintain significantly enhanced long-term stability. This stability underscores the intrinsic mutual coherence between the comb pairs, an essential requirement for effective dual-comb applications. Thus, the single-cavity dual-comb configuration offers a highly cost-effective solution, eliminating the necessity for complex

#555772 https://doi.org/10.1364/OE.555772
Journal © 2025 Received 17 Jan 2025; revised 14 Mar 2025; accepted 15 Mar 2025; published 16 Apr 2025

Optics EXPRESS

stabilization techniques such as Pound-Drever-Hall (PDH) locking or electronic phase-locked loop methods.

Other advantages of generating both combs in the same cavity include the ability to control the repetition rate difference between them [12] and the general possibility of designing the system so that both combs have the same optical bandwidth. This is a necessary condition for most applications.

However, dual-comb generation using single cavity laser technique systems face several challenges that need to be addressed, namely short-term and long-term stabilities. In the short-term stability the coherence between the combs must be even greater and the difference in the variation of the f_{CEO} and f_{rep} of comb 1 compared to the variation of the f_{CEO} and f_{rep} of comb 2 should be almost non-existent. In the long-term stability the system should maintain a dual comb regime for very long periods, thousands of hours, so that these systems can be used for commercial applications. This is always a challenge in the case of fiber lasers.

When it comes to the methods of single-cavity dual-comb generation, there are up to four different ones by which it can be achieved. These methods are: wavelength division, polarization, circulation direction and cavity space. These methods can be used individually or in combinations with one another [13]. Though the most published research in the field of single-cavity dual comb generation is demonstrated in fiber lasers, it can also be achieved in free-space cavities [14].

In this paper, we demonstrate a dual-comb polarization-multiplexing ring-cavity fiber laser system tailored for precision ranging applications with improved short-term and long-term stability capable of operating for over 125 hours for the first time, paving the way towards the industrial use of single-cavity dual-comb fiber lasers.

2. Setup and fundamental characteristics

Among the various options for generating two combs in the same cavity, polarization multiplexing stands out as one of the most suitable. Due to the nature of this method, both combs share most of the optical bandwidth but at the same time they can be separated using their polarization differences [12]. Thus, their noise is shared and can be mutually excluded.

Utilizing insights from previous laser cavity designs [12,13], we constructed the cavity illustrated in Fig. 1. This cavity, with a total length of 5.25 m, includes a Wavelength Division Multiplexing (WDM) component at the input, which combines the continuous wave pump light at 980 nm with the pulses already circulating within the cavity at approximately 1560 nm. The cavity also contains a 45 cm segment of Er^{3+}-doped fiber (ER110-4/125), a 0.5 m PM-1550 fiber, and a 51 dB dual-stage polarization-independent optical isolator (Thorlabs IOT-H-1550A). Additionally, it features a polarization controller, a single-wall carbon nanotube (CNT) absorber of the film type, and an output fiber coupler that directs 25% of the light outside the cavity. The fundamental repetition rate is 39.25 MHz, corresponding to a round-trip time of 25.47 ns. The entire cavity has a net anomalous GVD of –0.0201 ps^2/km, and the typical output power is 0.3 mW. The laser system is housed in a custom-made enclosure, laser-cut from transparent polycarbonate plastic, with multiple 3D-printed holders used to support and secure the optical fibers and components.

The output of the cavity is split using a combination of a Polarization Controller (PC) and a Polarization Beam Splitter (PBS). Both fast and slow combs are separated with an extinction ratio of 18.05 dBm for the fast axis and 17.9 dBm for the slow axis (see Fig. 2(a)). This separation level leads to the OSA Spectrums shown in Fig. 2(b). Out of these spectrums, we calculate a central wavelength, of 1559.78 nm for the fast axis, 1559.455 nm for the slow axis, and 1559.46 nm for the combined optical spectrum. At the same time, their FWHM broadband frequencies are $\Delta\lambda_{fast}$ = 1.836 nm for the fast axis, $\Delta\lambda_{slow}$ = 1.838 nm for the slow axis, and $\Delta\lambda_{Original}$ = 1.838 nm for the original comb. Once both combs have been separated and their pulse trains are divided into reference, target on the one hand, and local oscillator on the other. The fast axis

Optics EXPRESS

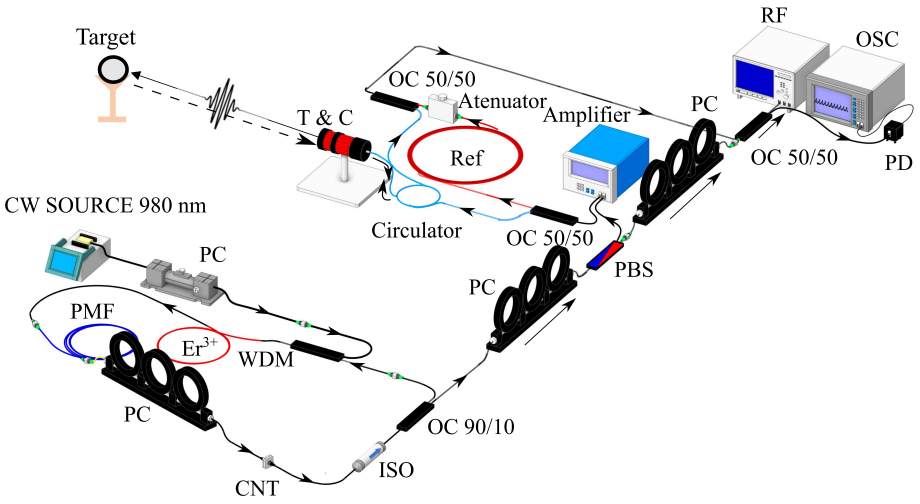

Fig. 1. Representation of the laser cavity and the lidar system. polarization controller (PC), polarization beam splitter (PBS), optical coupler 50/50 (OC), circulator, collimator telescope (T&C), a segment of referent fiber (Ref) and an attenuator. The amplifier is used just for the telescope and reference part. In combination with a photodiode (PD), an optical spectrum analyzer (OSA), and a radio frequency spectrum analyzer (RF). The black arrows represent the flow of light.

is amplified and subdivided using a 50/50 Optical Coupler (OC). 50% of the signal is directed towards the target, while the other 50% is sent to the reference. A telescope is aligned with the target, whereas the reference path consists of a segment of fiber of a known length that includes an attenuator. The attenuator is used to match the optical power of the target and reference signals. Without this, one signal might dominate the other, and the noise from the more powerful signal could obscure the weaker one. In some cases, instead of using a telescope to send and receive the signal from the target, a segment of fiber is used to avoid optical power losses. Finally, the signal polarized along the slow axis, acting as a local oscillator, is passed through a PC and then combined in a 50/50 optical coupler. Both signals are mixed in a photodetector, and the resulting signal is measured using a 32 GHz high-performance sampling oscilloscope (Agilent DSOX93204A Infinium) and the RF spectrum analyzer. The photodetector used for the OSC is a slow photodetector DC-125 MHz and it works in combination with a low band pass filter capped at 15 MHz. This filter helps increasing the SNR of the signal in the heterodyne detection and therefore helps extract the values of distance with more precision.

3. Results and discussion

The results presented in this work include stability analyses, which are divided into short-term and long-term stability results, as well as ranging results obtained using the complete setup shown in Fig. 1.

3.1. Long-term stability

In terms of RF spectrum stability, we observe behavior similar to the results shown in [12,15] when evaluating the Δf_{rep} stability over an extended period, now measured over 125 hours. Initially, during the first 53.5 hours, the frequency difference between the combs progressively increases at a rate of 0.6257 Hz per hour, rising from 1108.725 Hz to 1142.2 Hz. This is followed by a decreasing phase over 20 hours, during which the frequency difference drops to less than

Optics EXPRESS

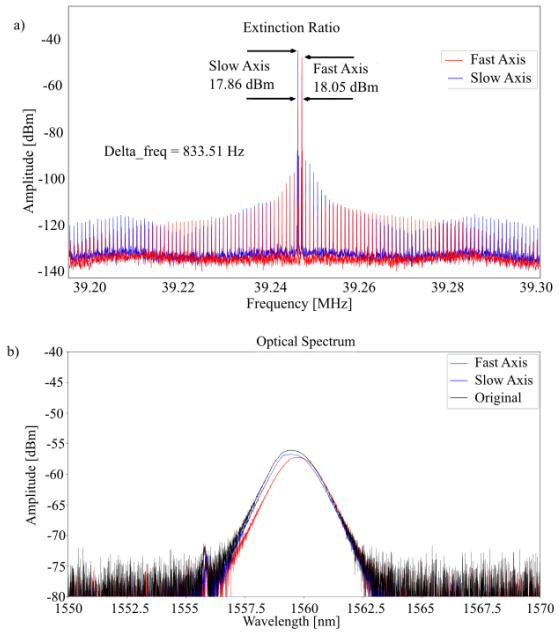

Fig. 2. Comb separation. (a) RF spectrum of the fast (red) and slow (blue) axis with their respective extinction ratios after separation. (b) OSA spectrum of the fast (red) and slow (blue) and the original signal (black).

1125.5 Hz. The highest drift deviation occurs over a 4-hour period, reaching 2 Hz per hour. The main source of the drift is likely temperature, as suggested by preliminary observations and general reasoning, although a thorough study has not yet been conducted to confirm this. The modifications made to the laser setup, compared to our previous demonstrations [12,15], have significantly improved stability by a factor of 17, extending it from 7 hours to 125 hours. These modifications are discussed in the section 3.2. Notably, stabilities of up to 250 hours have been observed, which is a significant improvement compared to other works in the literature, where stability is typically maintained for only 1 to 2 hours [16–20].

Figures 3(a) and 3(b) illustrate the spectral and frequency stability of the laser used in this work. Both vector solitons coexist for over 125 hours, although with notable fluctuations influenced by external temperature variations. The OSA stability results indicate an initial phase of instability within the first 150 minutes, followed by a stable phase (Fig. 3(a)). However, towards the end, the OSA spectrum experiences significant instability. Typically, optical spectra stability is the best indicator of long-term stability in the dual-comb regime, nonetheless changes in the spectrum does not necessarily mean changes in the Δf_{rep}.

Figure 3(b) presents the results for dual-comb temporal stability, specifically for dual-comb operation with a repetition rate difference of 1100 Hz. The dual-comb was monitored for 125 hours at room temperature, and the regime remained consistent after that period, with a slight shift in repetition rate and central wavelength. Despite some drift in the carrier-envelope offset frequency, the offset between the two combs shows stability with a drift of 1 Hz per hour, ranging from 1120 Hz to 1150 Hz without any additional external stabilization. The resolution bandwidth (RBW) of the RF spectrum analyzer was 1 Hz. To further reduce the Δf_{rep} drift in the future, mechanisms such as injection locking may be suited for this type of cavity [21,22].

Optics EXPRESS

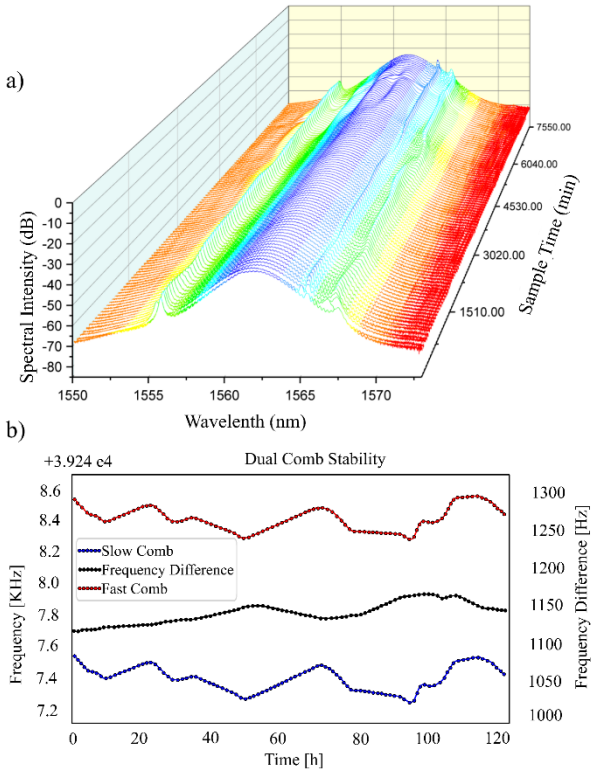

Fig. 3. Dual comb stability over time. (a) Optical spectra stability. (b) Dual comb Δ_{frep} stability over time.

3.2. *Short-term stability*

Using DFT in a similar way to the one done in our previous work [15] we obtained the intensity dynamics presented in Fig. 4. These results show that the mode-locking of both combs is stable and pure from round trip to round trip since the lines are straight and keep the shape. It can also be appreciated that one of the lines moves away from the other, meaning that one of the combs travels slightly faster than the other within the round trip. In fact, the exact round trip time of the fast axis is 25.480056 ns while for the slow axis, it is 25.479543 ns. It results in a round trip difference of 513 fs. Unstable shapes or broadening and narrowing of the lines would have meant that the mode-locking is unstable, nonetheless, that doesn't appear in this regime, giving another proof of its stability. In this case of its short-term stability.

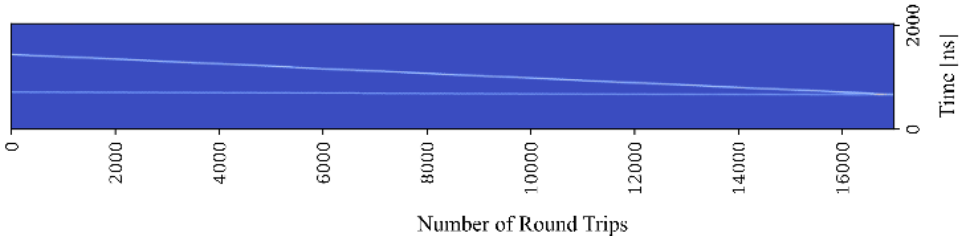

Fig. 4. Intensity dynamics of the dual-comb regime obtained using dispersive Fourier transform over a period of 17000 roundtrips

Optics EXPRESS

Additionally, the refractive indexes to be $n_{slow} = 1.454973$ and $n_{fast} = 1.45494112$ for the slow and fast axes, respectively. The refractive index difference is n_{slow} - $n_{fast} = \Delta n = 3.188 \times 10^{-5}$. So, the difference in the propagation constant $\Delta\beta = 128.5\ m^{-1}$, the beat length $L_B = 0.0489$ m, and the phase delay $\Delta\varphi = 674.546$ rad can be found from the Eqs. (1, 2, and 3) as follows:

$$\Delta\beta = \frac{2\pi}{\lambda}\Delta n, \tag{1}$$

$$L_B = \frac{\lambda}{\Delta n} = \frac{2\pi}{\Delta\beta}, \tag{2}$$

$$\Delta\varphi = \Delta\beta L. \tag{3}$$

Figure 5(a) presents the RF phase noise measurement of the repetition rate of the laser cavity [23], highlighting significant improvements in the system's stability, compared to the previous work by Rodriguez Cuevas et al. [12]. Specifically, the phase noise has decreased from -70 dBc/Hz to -80 dBc/Hz at a 100 Hz offset frequency, indicating a quieter and more stable laser operation. These improvements are attributed to several modifications: reduction in total cavity length, decrease in gain media length while increasing doping levels, secure winding of optical fibers within 3D printed fiber treys to prevent displacement, and comprehensive isolation of components within a custom housing to mitigate external perturbations. Similar single-cavity schematics to the one presented here tend to show phase noise around the same range. For example, Kowalczyk et al. [18] also presented -80 dBc/Hz at a 100 Hz offset frequency while in their case the phase noise decreases more notably when they expand the offset frequency, and the effect of the beat notes disappears. In their case, their SNR is also around 60 dBm or quite like our case and the same happens with the Δf_{rep} drift that remains in the order of 2 Hz varying rapidly but remaining within these values over a 60 min sample.

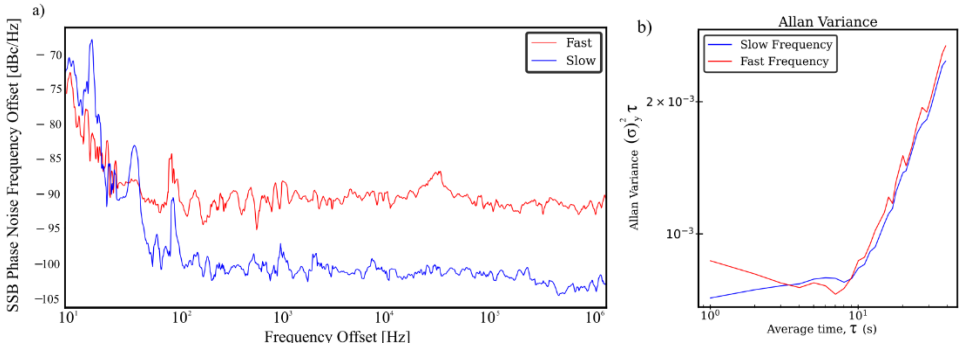

Fig. 5. (a) Short-term stability measurements. (a) RF phase noise. (b) Allan variance.

Figure 5(b) illustrates the Allan variance of the repetition rate, which is key metrics used to evaluate the stability of frequency sources over time. The Allan variance provides insights into the frequency stability of the repetition rate over various time intervals and indicates how the frequency of the laser changes over time. Allan variance is a statistical measure used to quantify the frequency stability of oscillators or frequency sources over various averaging times. It highlights the fluctuations in the signal by comparing the frequency differences between successive intervals. The data presented shows that the laser system maintains a frequency output typical of non-stabilized lasers (in the other of 10−3 Hz), or free running combs, as compared to stabilized OFCs that generate a single frequency comb and are available with stabilities in the order of 10−13 Hz for a second average time. Nonetheless, as it has been shown before, both combs drift together, and thus the mutual stability is superior to the individual of each comb. This stability is crucial for dual-comb applications.

Optics EXPRESS

3.3. Ranging results

The results presented in Fig. 6 correspond to the dual-comb ranging obtained using the scheme shown in Fig. 1. A 10 ms trace was captured with the fast oscilloscope (OSC) at a sampling rate of 40 MS/s (million samples per second), as shown in Fig. 6(a). Another 10 ms trace was captured using the same setup and oscilloscope but with the EF526 Low-Pass Electrical Filter ($\leq$ 15 MHz Passband) placed just before the oscilloscope. As shown in Fig. 6(b), the filter enhances the interferometric part of the signal by removing unwanted noise.. However, the signal is not as clean as reported in other publications [18,24], suggesting that further stabilization of the setup may be required. Despite this, the signal acquired in Fig. 6(b) allows us to extract the bursts corresponding to the target and the reference. The setup is configured so that the reference signal is always slightly larger than the target signal. Moreover, we accurately know the repetition rates of both signals. The signal processing involves identifying the highest point in the oscilloscope trace, corresponding to the most intense beating in the signal. We then select the remaining points at multiples of $1/f_{rep}$ to identify all bursts generated by the beating of the reference signal. A window of 6000 values before and after the point is created, and these points and their positions are extracted.

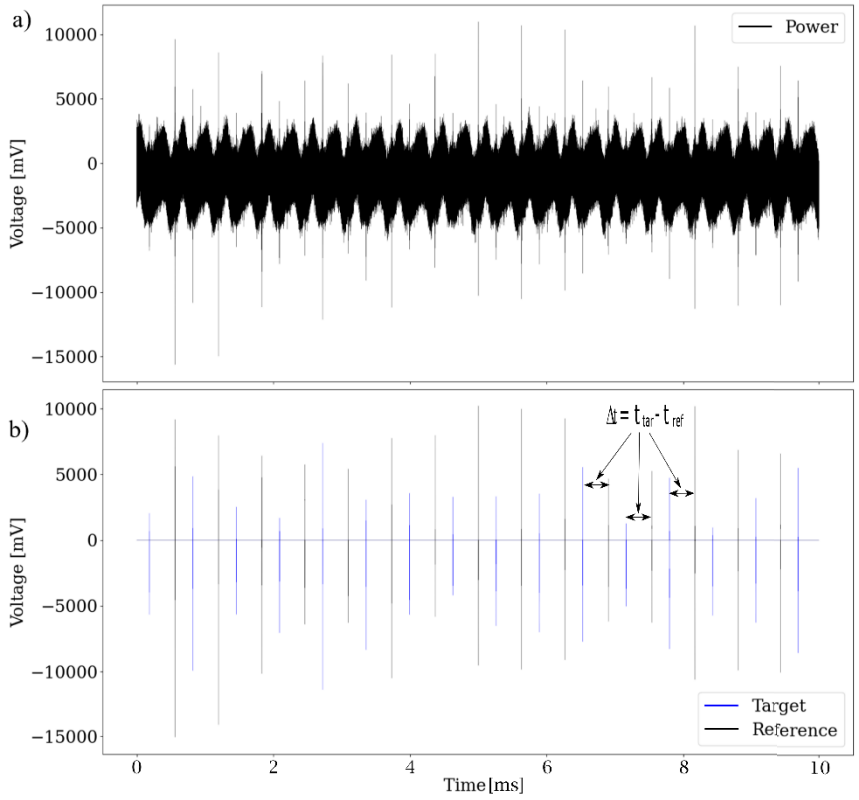

Fig. 6. OSC trace obtained from a dual-comb LIDAR scheme. (a) 10 ms OSC trace with a low band pass filter. (b) Post processed OSC trace from Fig. 6(a), in blue target echoes in black reference echoes.

We then perform a convolutional fitting of the interferograms with an example interferogram to accurately determine their central position. This central point serves as a reference, and we measure the temporal delay between the target and reference interferogram centres. These delays are then scaled using the oscilloscope's sampling rate, giving time delays between the

Optics EXPRESS

interferograms. To obtain the final distance values, we use the Eqs. (4) and 5.

$$\Delta t = \frac{1}{n}\sum_{i=1}^{n}(t_{tar,\ i} - t_{ref,\ i}), \tag{4}$$

$$D = \frac{\nu \cdot \Delta t}{2} \cdot \frac{\Delta frep}{f_{rep}} + D_{ref}. \tag{5}$$

In short, we multiply these time delays Δt that are extracted from the OSC trace by the conversion factor Δf_{rep} / f_{rep} and the speed of light in air, ν. Since the light pulse travels to the target and back, the resulting distance is divided by two. We add the reference distance, D_{ref}, and we can obtain the absolute distance to the target, D. By averaging over n number of values, being $n > 10$, we can obtain the mean distance and error as the standard deviation.

By applying this approach, we measured distances with a precision of 340 µm for a 10 ms averaging, a measured distance of 3073.905 mm, and an ambiguity range of 3.8 m. The first measurement corresponds to a fiber segment compared to a direct fiber connection without a telescope, as shown in Fig. 6(b). When free-space optics were used, the echoes from the target were weaker, leading to a lower signal-to-noise ratio (SNR).

This method is designed for future implementation using low-cost FPGA or microcontroller-based processing, similar to previous works [24,25], but adapted to single-cavity dual-comb sources. The current limitation in precision arises from not incorporating interferometric phase information. However, this can be mitigated by increasing the number of averaged values.

In conclusion, we designed a proof of concept for its use, successfully measuring distances of objects with sub-millimeter accuracy using a dual-comb polarization-multiplexing ring-cavity fiber laser. Our system demonstrated a high degree of both short-term and long-term stability, with the latter being particularly enhanced by modifications in the laser setup that extended stability to over 125 hours, a significant improvement over previous design. Though authors used the previously explored dual-comb technique, e.g., polarization multiplexing [26], the suggested approach can enable measurements of the polarimetric signatures of the target along with the distance. The preliminary results show that it can be realised by measuring polarization-multiplexed comb beatings for all Stokes parameters [12]. The ability of the dual-comb system to maintain coherence and stability over extended periods without external stabilization highlights its potential for practical applications in precision metrology and ranging. Future work may focus on further enhancing stability and exploring additional practical applications.

Funding. HORIZON EUROPE Marie Sklodowska-Curie Actions (ETN MEFISTA (861152)); Engineering and Physical Sciences Research Council (EP/W002868/1); Royal Academy of Engineering (IF2223B-133); Royal Society (IF\R1\241042RS).

Disclosures. No conflicts of interest, financial or otherwise, are declared by the authors.

Data availability. Data underlying the results presented in this paper are not publicly available at this time but may be obtained from the authors upon reasonable request.

References

1. H. R. Telle, G. Steinmeyer, A. E. Dunlop, *et al.*, "Carrier-envelope offset phase control: A novel concept for absolute optical frequency measurement and ultrashort pulse generation," Appl. Phys. B **69**(4), 327–332 (1999).
2. D. J. Jones, S. A. Diddams, J. K. Ranka, *et al.*, "Carrier-envelope phase control of femtosecond mode-locked lasers and direct optical frequency synthesis," Science **288**(5466), 635–639 (2000).
3. A. Apolonski, A. Poppe, G. Tempea, *et al.*, "Controlling the phase evolution of few-cycle light pulses," Phys. Rev. Lett. **85**(4), 740–743 (2000).
4. S. A. Diddams, D. J. Jones, J. Ye, *et al.*, "Direct link between microwave and optical frequencies with a 300 THz femtosecond laser comb," Phys. Rev. Lett. **84**(22), 5102–5105 (2000).
5. I. Coddington, W. C. Swann, L. Nenadovic, *et al.*, "Rapid and precise absolute distance measurements at long range," Nat. Photonics **3**(6), 351–356 (2009).
6. Z. Zhu and G. Wu, "Dual-Comb Ranging," Engineering **4**(6), 772–778 (2018).
7. I. Coddington, N. Newbury, and W. Swann, "Dual-comb spectroscopy," Optica **3**(4), 414 (2016).

Optics EXPRESS

8. T. Fortier and E. Baumann, "20 years of developments in optical frequency comb technology and applications," Commun. Phys. **2**(1), 153 (2019).
9. A. M. Zolot, F. R. Giorgetta, E. Baumann, *et al.*, "Direct-comb molecular spectroscopy with accurate, resolved comb teeth over 43 THz," Opt. Lett. **37**(4), 638–640 (2012).
10. Z. Chen, M. Yan, T. W. Hänsch, *et al.*, "A phase-stable dual-comb interferometer," Nat. Commun. **9**(1), 3035 (2018).
11. R. Liao, H. Tian, W. Liu, *et al.*, "Dual-comb generation from a single laser source: principles and spectroscopic applications towards mid-IR—A review," J. Phys. Photonics **2**(4), 042006 (2020).
12. A. R. Cuevas, H. J. Kbashi, D. Stoliarov, *et al.*, "Polarization dynamics, stability and tunability of a dual-comb polarization-multiplexing ring-cavity fiber laser," Results Phys. **46**, 106260 (2023).
13. X. Jin, R. Liu, J. Zhou, *et al.*, "Simultaneous generation of wavelength multiplexing and polarization multiplexing from a wavelength-tunable ultrafast fiber laser," Opt. Fiber Technol. **84**, 103719 (2024).
14. S. M. Link, D. J. H. C. Maas, D. Waldburger, *et al.*, "Dual-comb spectroscopy of water vapor with a free-running semiconductor disk laser," Science **356**(6343), 1164–1168 (2017).
15. A. Rodriguez Cuevas, I. Kudelin, H. Kbashi, *et al.*, "Single-shot dynamics of dual-comb generation in a polarization-multiplexing fiber laser," Sci. Rep. **13**(1), 19673 (2023).
16. X. Zhao, T. Li, Y. Liu, *et al.*, "Polarization-multiplexed, dual-comb all-fiber mode-locked laser," Photonics Res. **6**(9), 853–857 (2018).
17. Y. Nakajima, Y. Hata, and K. Minoshima, "All-polarization-maintaining, polarization-multiplexed, dual-comb fiber laser with a nonlinear amplifying loop mirror," Opt. Express **27**(10), 14648–14656 (2019).
18. M. Kowalczyk, L. Sterczewski, X. Zhang, *et al.*, "Dual-comb femtosecond solid-state laser with inherent polarization-multiplexing," Laser Photonics Rev. **15**(8), 2000441 (2021).
19. B. Willenberg, J. Pupeikis, L. M. Krüger, *et al.*, "Femtosecond dual-comb yb: Caf 2 laser from a single free-running polarization-multiplexed cavity for optical sampling applications," Opt. Express **28**(20), 30275–30288 (2020).
20. G. Hu, Y. Qin, Z. Zhou, *et al.*, "Repetition rate difference, stability and polarization extinction ratio of single-cavity polarization-multiplexed fiber laser with weak birefringence," Results Phys. **59**, 107563 (2024).
21. L. Shi, K. Ma, X. Ming, *et al.*, "Injection-locked soliton microcomb against temporal drifting," Results Phys. **54**, 107062 (2023).
22. D. A. Korobko, V. A. Ribenek, D. A. Stoliarov, *et al.*, "Resonantly induced mitigation of supermode noise in a harmonically mode-locked fiber laser: revealing the underlying mechanisms," Opt. Express **30**(10), 17243–17258 (2022).
23. R. Paschotta, A. Schlatter, S. C. Zeller, *et al.*, "Optical phase noise and carrier-envelope offset noise of mode-locked lasers," Appl. Phys. B **82**(2), 265–273 (2006).
24. H. Wright, J. Sun, D. McKendrick, *et al.*, "Two-photon dual-comb LiDAR," Opt. Express **29**(23), 37037–37047 (2021).
25. H. Wright, A. J. M. Nelmes, N. J. Weston, *et al.*, "Multi-target two-photon dual-comb LiDAR," Opt. Express **31**(14), 22497–22506 (2023).
26. B. Lin, X. Zhao, M. He, *et al.*, "Dual-Comb Absolute Distance Measurement Based on a Dual-Wavelength Passively Mode-Locked Laser," IEEE Photonics J. **9**(6), 1–8 (2017).